Plasmonic Focusing in Rod−Sheath Heteronanostructures

Xiaodong Chen,[§] Shuzhou Li,[§] Can Xue, Matthew J. Banholzer, George C. Schatz,* and Chad A. Mirkin*

Department of Chemistry and International Institute for Nanotechnology, Northwestern University, 2145 Sheridan Road, Evanston, Illinois 60208. [§]These two authors contributed equally to this work.

ABSTRACT This paper describes the fabrication of plasmonic focusing, free-standing rod−sheath heteronanostructures based on electrochemical templated synthesis and selective chemical etching. These heteronanostructures take advantage of plasmon interference together with field enhancements due to sharp junction structures to function as stand-alone SERS substrates containing Raman hot spots at the interface of the rod and sheath segments. This result is investigated with empirical and theoretical (discrete dipole approximation, DDA) methods, and we show how plasmon interference can be tuned by varying the sheath and rod lengths.

KEYWORDS: heteronanostructure · electrochemical deposition · SERS · plasmonics

Plasmonic nanostructures have been intensely studied because of their interesting fundamental properties and potential use as waveguides and enhancing structures in the context of metal-enhanced fluorescence and surface-enhanced Raman scattering (SERS).[1−4] Advances in nanofabrication are allowing researchers to probe the relationship between nanostructure and plasmonic properties. For example, electron-beam lithography has been used to fabricate metallic "bowtie" nanoantennas consisting of two opposing tip-to-tip Au triangles, which exhibit gap-dependent optical coupling.[5] Soft-lithography has been used to form arrays of nanoholes and nanoparticles which can be utilized for highly sensitive refractive index sensing.[6] Additionally, template-based methods such as nanosphere lithography[7] have been used to prepare periodic structures that exhibit large reproducible SERS properties, which may find utility in new chemical sensing schemes. Despite these achievements involving planar printing and lithographic methods, there are relatively few methods, which allow one to fabricate free-standing, dispersible nanostructures with control over feature size on the sub-100-nm length scale.

On-wire lithography (OWL), which is an emerging nanofabrication method based on the electrochemical deposition of multisegmented nanowires[8,9] and selective chemical etching of sacrificial segments, allows one to prepare a wide variety of nanowire-based structures with control over composition and both negative and positive architectural features along the long axes of the wires.[10] Researchers have used OWL to prepare electrodes with nanoscale gaps,[11,12] electrical nanotraps,[13] plasmonic disk arrays,[14] structures with optimized enhancing properties in the context of Raman spectroscopy,[15] and heterostructures that behave as catalytic nanorotors.[16] The technique is compatible with both soft and hard matter, and essentially any material that can be electrochemically plated or polymerized in a porous template can be deposited as a nanowire. Interestingly, when multisegmented wires, each made of a hard inorganic material like gold and a relatively soft polymeric material such as polypyrrole (PPy), remain in the template while they are dried under vacuum, the polymer segments will contract by about 10% and adhere to the side walls of the pores to form a crescent−shaped channel (Figure 1a). If gold is subsequently deposited into the channel, a novel rod−sheath structure is formed. Dissolution of the template and polymer results in the generation of approximately one billion of these dispersible rod−sheath nanostructures. Herein, we describe the detailed synthesis and characterization of this new class of heteronanostructure and the identification of a plasmonic focusing phenomenon that occurs at the point of contact between rod and sheath. Experimental observation of the focusing phenomenon as well as discrete dipole approximation (DDA) calculations aimed at understanding its origins are presented.

*Address correspondence to chadnano@northwestern.edu, schatz@chem.northwestern.edu.

Received for review October 17, 2008 and accepted November 25, 2008.

Published online December 9, 2008. 10.1021/nn800695u CCC: $40.75

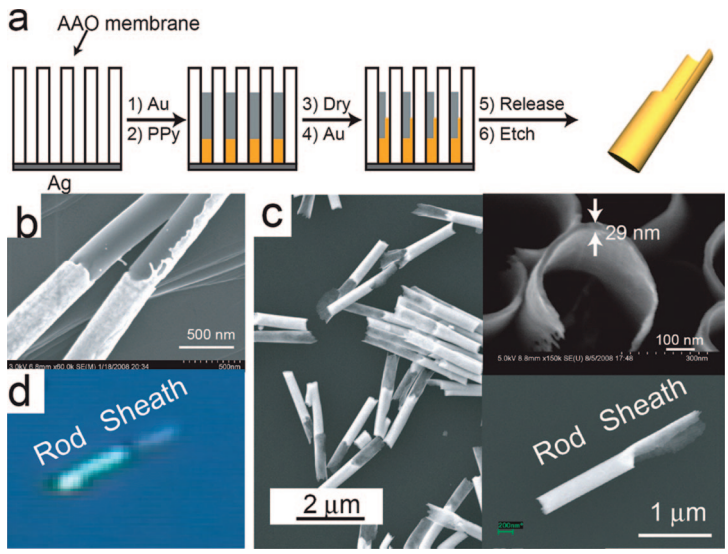

Figure 1. (a) Scheme illustrating the synthesis of Au rod−sheath heteronanostructures using a combination of electrochemical growth of metal−polymer nanorods in AAO membranes, followed by selective wet chemical etching of polymer. (b) SEM image of Au-PPy nanorods before chemical etching of the PPy segment. SEM images (c) and an optical image (d) of Au rod−sheath heteronanostructures (1.6 ± 0.2 μm length nanorod and 1.4 ± 0.3 μm sheath). The inset of panel c shows the thickness of the sheath (top) and an individual rod−sheath heteronanostructure (bottom).

RESULTS AND DISCUSSION

The strategy for making Au rod−sheath heteronanostructures involves the initial deposition of 200 nm of Ag onto one side of an anodic aluminum oxide (AAO) membrane to serve as the working electrode for subsequent electrochemical deposition of the rods (Figure 1a). Next, Au and PPy were sequentially deposited within the AAO template from Orotemp 24 RTU solution at −0.95 V *versus* Ag/AgCl and 0.25 M aqueous pyrrole and 0.1 M $LiClO_4$ at 0.75 V *versus* Ag/AgCl, respectively. Upon drying in vacuum, the PPy segment shrinks (approximately 30 nm) due to dehydration.[17] Because of the strong adhesion forces between the PPy and the inner pore walls of the AAO template, each PPy rod adheres to one side of the cylindrical pore, resulting in a small, curved channel. The deposition of additional gold into this structure (~0.5 C) results in a rod−sheath made of gold (Figure 1a,b). The electrostatic interaction between $[Au(CN)_2]^-$ and PPy rod surface may act as a driving force to replenish gold ion in the volume that eventually becomes the sheath.[18] Finally, the Ag backing layer was removed by dissolution in a solution of methanol, 30% ammonium hydroxide, and 30% hydrogen peroxide (4:1:1, v/v/v). The alumina template was dissolved in 3 M NaOH. During these steps, the PPy segments were also removed. The formation of the rod−sheath nanostructures was confirmed by scanning electron microscopy (SEM) (Figure 1c). The thickness of the sheath is 28 ± 3 nm, which is approximately the diameter difference between the Au rods and contracted PPy nanorods.[17] Optical microscopy (Figure 1d) can be used to differentiate the rod and sheath ends, since they exhibit different degrees of light scattering.

Since the shape of a nanostructure plays an important role in its plasmonic properties,[2] we investigated the surface-enhanced Raman scattering (SERS) behavior of the obtained novel rod−sheath heteronanostructures. SERS is directly related to the electromagnetic field profile ($|E|^4$) of a nanostructure, so a map of SERS activity along the nanowire can serve as a good indication of electromagnetic field intensity. The rod−sheath heteronanostructures (1.6 ± 0.2 μm length nanorod and a sheath end varying from 0.8 to 1.8 μm in length) were functionalized with methylene blue (MB) and subsequently characterized by confocal Raman and conventional bright-field microscopy (WiTec Alpha300). Samples were excited using a He−Ne laser (632.8 nm, Coherent Inc., Santa Clara, CA) with ~0.1 mW intensity. The confocal Raman images (Figure 2a,b) were obtained by integrating the spectral intensity from 1600 to 1700 cm^{-1}, where 1630 cm^{-1} corresponds to the mode of C−C ring stretching of MB.[19] It is interesting to observe that, with a rod length of ~1.7 μm and a sheath length of ~1.5 μm, the intensity of the Raman signal at the junction formed between rod and sheath segments is over ~4 times higher than that at the edge of the rod or sheath (which are known to already be highly enhancing themselves) (Figure 2c). This finding suggests a strong electromagnetic field at the junction of the rod and sheath segments. To investigate whether the Au sheath plays an important role in generating this strong electromagnetic field, we also fabricated a Au−SiO_2 rod−sheath heteronanostructure of similar dimensions (Figure 3 and Figure S2b) through the OWL technique.[10] This involves creating gold−nickel two-segmented nanorods by template-directed electrochemical synthesis. After coating one side of these two-segmented rods with 50 nm of silica through

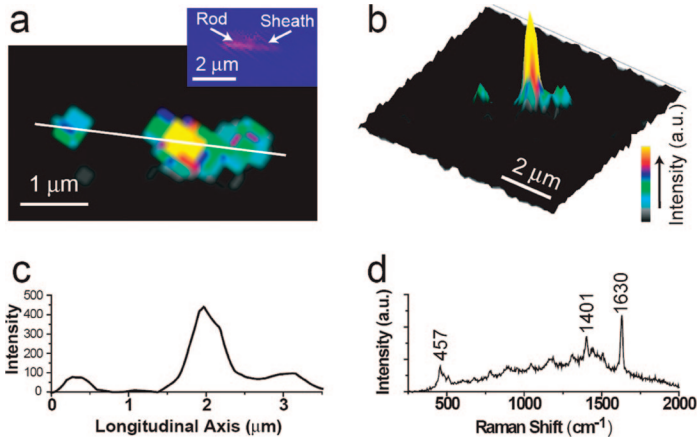

Figure 2. 2D (a) and 3D (b) confocal scanning Raman images of rod−sheath heteronanostructures (rod: ~1.7 μm; sheath: ~1.5 μm) modified by MB. Optical image (inset of panel a), which is simultaneously obtained, shows the orientation of the nanostructures. (c) Cross-section of the Raman intensity *vs* the location along the longitudinal axis of the rod−sheath nanostructures (white line in a). (d) Representative Raman spectrum of MB taken from the center of the hot spot shown in the Raman maps.

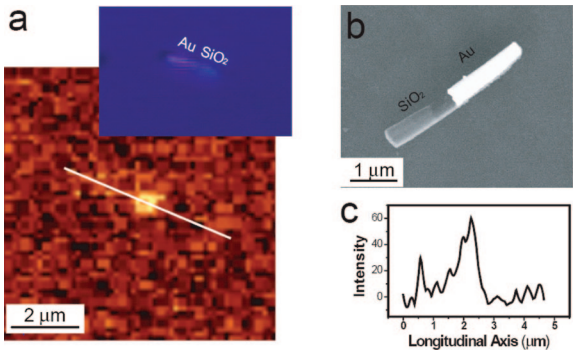

Figure 3. (a) 2D confocal scanning Raman image of Au−SiO_2 rod−sheath heteronanostructures modified by MB (the observed MB spectra for this sample is similar to the one shown in Figure 2d). Optical image (inset of a), which is simultaneously obtained, clearly shows the orientation of the nanostructures. (b) SEM image of Au-SiO_2 rod−sheath heteronanostructures fabricated by OWL. (c) Cross-section of the Raman intensity *vs* the location of the longitudinal axis of the rod−sheath nanostructures (white line in a).

plasma-enhanced vapor chemical deposition (PEVCD), the ~1.5 μm nickel segment is removed by selective wet-chemical etching, resulting in heteronanostructures consisting of ~1.6 μm Au rods and ~1.5 μm SiO_2 sheaths (Figure 3b). Finally, the Au−SiO_2 rod−sheath heteronanostructures were functionalized with MB for Raman measurements. Significantly, the intensity of Raman signal at the contact junction of Au rod and SiO_2 sheath is quite similar to that at the edge of Au rod (Figure 3a,c), suggesting that the metal−metal junction is important in generating the enhanced electromagnetic fields.

To further understand the plasmonic features of these rod−sheath systems, we systematically investigated the SERS behavior of rod−sheath heteronanostructures with different sheath lengths but similar rod sizes (1.6 ± 0.2 μm). Interestingly, we found a pseudosinusoidal relationship between the sheath length and the ratio of hot spot intensity localized around rod−sheath junction to that at the rod end (Figure 4a). For example, with sheath lengths of ~1.3 and ~1 μm, the intensity localized around the junction relative to the rod ends is low. However, for ~1.5 and ~1.2 μm sheaths, the intensity of the Raman signal at the junction of rod and sheath segments of the nanowire is much greater than at the rod ends.

To interpret the observed results, we have calculated the local electric fields for the Au rod−sheath heteronanostructures in vacuum using DDA methods.[20,21] Here, we only consider the light polarization parallel to the longitudinal axis of the rod−sheath heteronanostructure since the coupling of two plasmonic structures (such as for dimers in our previous work[7]) is most important for light polarized along the dimer axis.[22] The grid spacing is 5 nm in all calculations, and the gold dielectric constants are from Johnson and Christy.[23] As one example of such a calculation, Figure 5a presents the resulting contour of $|E|^2$ for a rod−sheath nano-

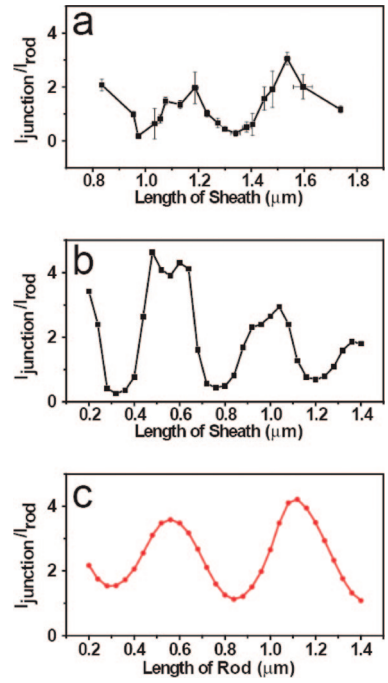

Figure 4. (a) Experimental data of the ratio of hot spot intensity localized around rod−sheath conjunction to that at the rod end as a function of the sheath length. Rod length: 1.6 ± 0.2 μm. (b) DDA calculation of the ratio of hot spot intensity at the rod−sheath conjunction to that at the rod end as a function of the sheath length while keeping the rod length at 1 μm. (c) DDA calculation of the ratio of hot spot intensity at the rod−sheath conjunction to that at the rod end as a function of the rod length while keeping the sheath length 1 μm. The field enhancement is modeled at 633 nm radiation for a Au nanostructure with the following geometry: diameter of rod, 360 nm; thickness of sheath, 30 nm; and grid spacing, 5 nm.

structure excited at 633 nm, where E is the electric field. In this nanostructure, the length and the diameter of the rod are 1000 and 360 nm, respectively. The sheath is 1000 nm in length and 30 nm in thickness. In Figure 5b the SERS enhancement factor ($\int|E|^4 ds$) of the nanostructure is plotted as a function of location along the longitudinal axis. It is found that the magnitude of the SERS enhancement factor is about 3 times larger at the rod/sheath interface than at the edge of the rod or sheath, which is in good agreement with our observed results (Figure 2c). The peaks in the experiments are much broader than those in calculations, which is due to the lower spatial resolution and heterogeneity in experiments.

We also calculated electromagnetic enhancement factors for the individual rod and sheath nanostructures, and plotted their intensity profiles as a function of location along the longitudinal nanostructure axis (Figure 5c,d). Both rods and sheaths show high electric fields at their ends, corresponding to the influence of the sharp nanostructures ("lightning rod-effect") on the local fields. For individual rods, the intensity is similar to that at the edge of the rods in the heteronanostructures. However, the calculations show that the SERS enhancement factor on the sheath end of the heteronano-

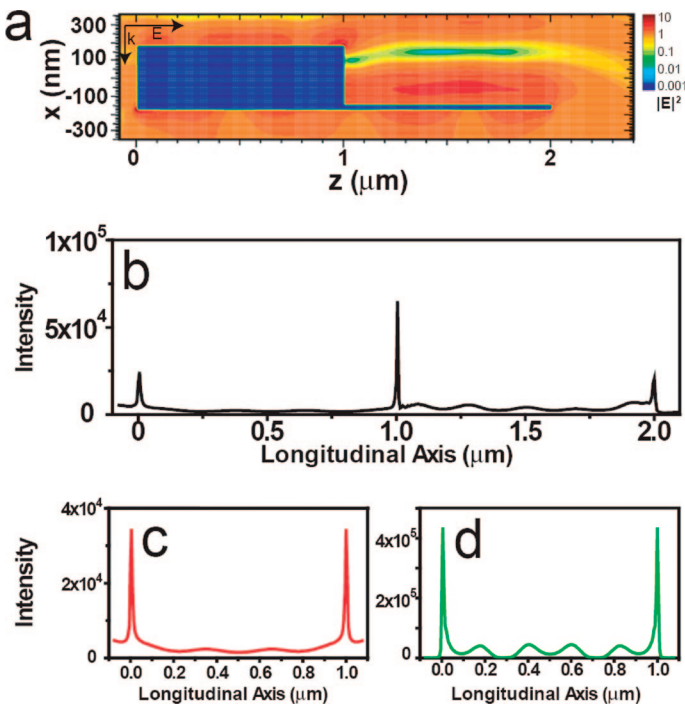

Figure 5. (a) Electric field contour ($|E|^2$) of the Au rod−sheath nanostructure calculated with DDA in vacuum. The $\int |E|^4 ds$ intensity profile along the longitudinal axis is plotted for the rod−sheath nanostructure in panel b, the individual rod in panel c, and the individual sheath in panel d. The field enhancement is modeled at 633 nm radiation for a Au nanostructure with the following geometry: rod, 1 μm; sheath, 1 μm; diameter of rod, 360 nm; thickness of sheath, 30 nm; and grid spacing, 5 nm.

structure is significantly smaller than the sheath alone, while that at the junction is larger than the edge of the rods. A possible reason for the increase for the heteronanostructure is that the heteronanostructure is closer to resonance at 633 nm than each of the separate structures because of coupling between the rod and sheath. Figure S3 shows the extinction spectra for rods, sheaths, and heteronanostructures, and we see that there is no resonance around 633 nm for the rod, while the sheath resonances are near 633 nm, and the heteronanostructure is in-between. However, a close inspection of rod−sheath structure's intensity profiles along the symmetry axis shows the peak intensity around the junction is not closely correlated to the resonance positions of the whole nanostructure, which is shown in Figure S4. Another reason for the enhanced intensity in the heteronanostructure is that the enhancement at the junction of two structures, such as for homodimers as studied in earlier work,[15,24] is significantly higher than for each separate structure. Indeed in some past work[25,26] the term "superfocusing" has been used to describe this phenomenon. The intensity profiles (Figure 5) also clearly show interference fringes associated with propagating surface plasmon polaritons (SPPs)[27] in the sheath with an interference period of ~210 nm (corresponding to $\lambda_{SPP}/2$). This suggests that the electromagnetic energy of the SPPs is enhanced at the junction of rod and sheath segments as a result of interference of SPPs in the rod and sheath.

Further DDA calculations for the different sheath lengths while keeping the rod segment constant also reveal an interesting, pseudosinusoidal relationship between sheath length and the observed intensity at the junction (Figure 4b). The period of the enhancement factors in this calculation (~400 nm) is in good agreement with that of the measured SERS intensity oscillations (Figure 4a). The theory and experimental oscillations are slightly out of phase with each other, probably as a result of differences between the chosen rod lengths in the simulations (1000 nm) and experiments (1700 nm). Note that the 400 nm value for λ_{SPP} is smaller than the 600 nm value usually quoted for an infinitely thick gold film[21] for 633 nm excitation wavelength due to the finite thickness of the film. Indeed, an SPP wavelength of 410 nm can be estimated for flat 15 nm films based on results in ref 28. The wavelength might further be modified for a sheath due to curvature effects.

One further point is why the oscillations in Figure 4 are λ_{SPP} rather than $\lambda_{SPP}/2$. Generally one would expect that $|E|^2$ (or $|E|^4$) would have $\lambda_{SPP}/2$ periodicity for the stationary SPP modes of a rod or film;[29] however, in past work[30] it was demonstrated that λ_{SPP} periodicity can result from interference between the incident plane wave and the SPP modes of thin metal films. This same interference should apply to the rod/sheath structure, thus explaining the λ_{SPP} periodicity. However note that λ_{SPP} periodicity should even apply to Figure 5 where the periodicity seemed to be $\lambda_{SPP}/2$. Upon careful inspection of this figure, it is clear that the periodicity is actually λ_{SPP}, with a relatively strong, but not quite periodic structure at $\lambda_{SPP}/2$ due to weak interference of the SPP with the applied plane wave field. In Figure 4c, the enhancement factor at the junction is plotted as a function of rod length. Here the sheath length was fixed at 1000 nm. The period in Figure 4c is around 600 nm, which is close to the infinite film thickness value of λ_{SPP}. This is reasonable since the diameter of rod is 360 nm, which is much larger than the penetration depth of the SPP on gold films.

CONCLUSIONS

In this work, we have shown experimentally and theoretically that these novel rod−sheath nanostructures exhibit a significant electromagnetic enhancement at the junction between rod and sheath and that interference of the SPPs combined with field enhancement at the junction is responsible for such enhancement. Moreover, we show that OWL can be used to produce an entire family of these structures with different relative lengths to understand the origin of plasmonic focusing. Surface plasmonic focusing can be used potentially in a variety of systems, including plasmonic waveguides,[1] plas-

monic lithography,[31] and proposed terahertz photonic devices.[32] Corrugated or conical nanostructures,[25,26,33−35] prepared by planar and resolution-limited conventional lithographic tools, are typically used for superfocusing in the aforementioned applications. Therefore, the free-standing rod−sheath heteronanostructures reported herein represent a new type of nanostructure for focusing.

METHODS

Materials. Multisegment nanowires were prepared according to literature methods.[10] 200 nm of Ag metal was evaporated on the back of anodic aluminum oxide (AAO) membranes (Whatman, Anodisc 0.02 μm pores, 47 mm outer diameter). These membranes were then placed in an electrochemical cell, which contained a Pt counter electrode and an Ag/AgCl reference electrode. In all experiments, commercially available 1025 silver (Ag) and nickel sulfamate RTU (Ni), Orotemp 24RTU (Au) electroplating solutions (Technic Inc.) were used for electrochemical deposition. The total charge passed during deposition determined the desired nanowire structure. Ag was deposited as an initial electrical contact layer under DC current at −800 mV (*versus* Ag/AgCl), while gold was plated at −950 mV. PPy was deposited within the AAO template from mixed aqueous solution of 0.25 M pyrrole and 0.1 M lithium perchlorate at 0.75 V *versus* Ag/AgCl. Pyrrole, lithium perchlorate, hydrogen peroxide, methanol, ammonium hydroxide, sodium hydroxide, and methylene blue were purchased from Sigma.

Characterization. Scanning electron microscopy (Hitachi S4800) was used for morphology measurements. Raman spectra were recorded with a confocal Raman microscope (Alpha300 WiTec) equipped with a piezo scanner and 100× microscope objectives (n.a. = 0.90; Nikon, Tokyo, Japan). Samples were excited with a 632.8-nm He−Ne laser (Coherent, Inc., Santa Clara, CA) with a power density of $\sim 10^4$ W/cm^2 and were excited with the long axis of the nanostructure parallel to the laser polarization.

Theoretical Modeling. Local electric fields and extinction spectra for the Au rod−sheath heteronanostructures were calculated using discrete dipole approximation (DDA) methods in vacuum.[20,21] Here, we only consider the light polarization parallel to the longitudinal axis of the rod−sheath heteronanostructure since the coupling of the two plasmonic structures is most important for light polarized along the dimer axis. The grid spacing is 5 nm in all calculations and the gold dielectric constants are from Johnson and Christy.[23] The incident wavelength used in the calculation is chosen to be the excitation wavelength of 633 nm in what we present. The magnitude of incident light is 1. The SERS enhancement factor equals $|E_L/E_0|^4$, where E_L and E_0 are the local field and incident field, respectively.[36]

Acknowledgment. C.A.M. and G.C.S. acknowledge support from AFOSR, NSF-NSEC, and DARPA. C.A.M. is also grateful for an NIH Director's Pioneer Award and an NSSEF Fellowship from the Department of Defense.

Supporting Information Available: Theoretical calculation of extinction spectra and hot spot intensity data for rod, sheath, and rod−sheath nanostructures. This material is available free of charge *via* the Internet at http://pubs.acs.org.

REFERENCES AND NOTES

1. Ozbay, E. Plasmonics: Merging Photonics and Electronics at Nanoscale Dimensions. *Science* **2006**, *311*, 189–193.
2. Banholzer, M. J.; Millstone, J. E.; Qin, L. D.; Mirkin, C. A. Rationally Designed Nanostructures for Surface-Enhanced Raman Spectroscopy. *Chem. Soc. Rev.* **2008**, *37*, 885–897.
3. Wang, H.; Brandl, D. W.; Nordlander, P.; Halas, N. J. Plasmonic Nanostructures: Artificial Molecules. *Acc. Chem. Res.* **2007**, *40*, 53–62.
4. Henzie, J.; Lee, J. H.; Lee, M. H.; Hasan, W.; Odom, T. W. Nanofabrication of Plasmonic Structures. *Annu. Rev. Phys. Chem.* **2009**, *60*, 147–165.
5. Fromm, D. P.; Sundaramurthy, A.; Schuck, P. J.; Kino, G.; Moerner, W. E. Gap-Dependent Optical Coupling of Single "Bowtie" Nanoantennas Resonant in the Visible. *Nano Lett.* **2004**, *4*, 957–961.
6. Henzie, J.; Lee, M. H.; Odom, T. W. Multiscale Patterning of Plasmonic Metamaterials. *Nat. Nanotechnol.* **2007**, *2*, 549–554.
7. Haynes, C. L.; Van Duyne, R. P. Nanosphere Lithography: A Versatile Nanofabrication Tool for Studies of Size-Dependent Nanoparticle Optics. *J. Phys. Chem. B* **2001**, *105*, 5599–5611.
8. Hurst, S. J.; Payne, E. K.; Qin, L. D.; Mirkin, C. A. Multisegmented One-Dimensional Nanorods Prepared by Hard-Template Synthetic Methods. *Angew. Chem., Int. Ed.* **2006**, *45*, 2672–2692.
9. Martin, C. R. Nanomaterials—A Membrane-Based Synthetic Approach. *Science* **1994**, *266*, 1961–1966.
10. Qin, L. D.; Park, S.; Huang, L.; Mirkin, C. A. On-Wire Lithography. *Science* **2005**, *309*, 113–115.
11. Qin, L. D.; Jang, J. W.; Huang, L.; Mirkin, C. A. Sub-5-nm Gaps Prepared by On-Wire Lithography: Correlating Gap Size with Electrical Transport. *Small* **2007**, *3*, 86–90.
12. Chen, X. D.; Jeon, Y.-M.; Jang, J.-W.; Qin, L. D.; Huo, F. W.; Wei, W.; Mirkin, C. A. On-Wire Lithography-Generated Molecule-Based Transport Junctions: A New Testbed for Molecular Electronics. *J. Am. Chem. Soc.* **2008**, *130*, 8166–8168.
13. Zheng, G. F.; Qin, L. D.; Mirkin, C. A. Spectroscopically Enhancing Electrical Nanotraps. *Angew. Chem., Int. Ed.* **2008**, *47*, 1938–1941.
14. Qin, L. D.; Banholzer, M. J.; Millstone, J. E.; Mirkin, C. A. Nanodisk Codes. *Nano Lett.* **2007**, *7*, 3849–3853.
15. Qin, L. D.; Zou, S. L.; Xue, C.; Atkinson, A.; Schatz, G. C.; Mirkin, C. A. Designing, Fabricating, and Imaging Raman Hot Spots. *Proc. Natl. Acad. Sci. U.S.A.* **2006**, *103*, 13300–13303.
16. Qin, L. D.; Banholzer, M. J.; Xu, X. Y.; Huang, L.; Mirkin, C. A. Rational Design and Synthesis of Catalytically Driven Nanorotors. *J. Am. Chem. Soc.* **2007**, *129*, 14870–14871.
17. Ciszek, J. W.; Huang, L.; Wang, Y. H.; Mirkin, C. A. Kinetically Controlled, Shape-Directed Assembly of Nanorods. *Small* **2008**, *4*, 206–210.
18. Hernandez, R. M.; Richter, L.; Semancik, S.; Stranick, S.; Mallouk, T. E. Template Fabrication of Protein-Functionalized Gold−Polypyrrole−Gold Segmented Nanowires. *Chem. Mater.* **2004**, *16*, 3431–3438.
19. Naujok, R. R.; Duevel, R. V.; Corn, R. M. Fluorescence and Fourier-Transform Surface-Enhanced Raman-Scattering Measurements of Methylene-Blue Adsorbed onto a Sulfur-Modified Gold Electrode. *Langmuir* **1993**, *9*, 1771–1774.
20. Draine, B. T.; Flatau, P. J. User Guide to the Discrete Dipole Approximation Code DDSCAT 6.1.arXiv.org e-Print archive; http://Arxiv.Org/Abs/Astro-Ph/0409262v2, arXiv:0409262v2, 2004.
21. Kelly, K. L.; Coronado, E.; Zhao, L. L.; Schatz, G. C. The Optical Properties of Metal Nanoparticles: The Influence of Size, Shape, and Dielectric Environment. *J. Phys. Chem. B* **2003**, *107*, 668–677.
22. Lassiter, J. B.; Aizpurua, J.; Hernandez, L. I.; Brandl, D. W.; Romero, I.; Lal, S.; Hafner, J. H.; Nordlander, P.; Halas, N. J. Close Encounters Between Two Nanoshells. *Nano Lett.* **2008**, *8*, 1212–1218.
23. Johnson, P. B.; Christy, R. W. Optical-Constants of Noble-Metals. *Phys. Rev. B* **1972**, *6*, 4370–4379.

24. Gunnarsson, L.; Rindzevicius, T.; Prikulis, J.; Kasemo, B.; Kall, M.; Zou, S. L.; Schatz, G. C. Confined Plasmons in Nanofabricated Single Silver Particle Pairs: Experimental Observations of Strong Interparticle Interactions. *J. Phys. Chem. B* **2005**, *109*, 1079–1087.
25. Atay, T.; Song, J. H.; Nurmikko, A. V. Strongly Interacting Plasmon Nanoparticle Pairs: From Dipole−Dipole Interaction to Conductively Coupled Regime. *Nano Lett.* **2004**, *4*, 1627–1631.
26. Lalayan, A. A.; Bagdasaryan, K. S.; Petrosyan, P. G.; Nerkararyan, K. V.; Ketterson, J. B. Anomalous Field Enhancement From the Superfocusing of Surface Plasmons at Contacting Silver Surfaces. *J. Appl. Phys.* **2002**, *91*, 2965–2968.
27. Barnes, W. L.; Dereux, A.; Ebbesen, T. W. Surface Plasmon Subwavelength Optics. *Nature* **2003**, *424*, 824–830.
28. Raether, H. *Surface Plasmons on Smooth and Rough Surface and on Gratings*; Springer: New York, 1986.
29. Kwak, E. S.; Henzie, J.; Chang, S. H.; Gray, S. K.; Schatz, G. C.; Odom, T. W. Surface Plasmon Standing Waves in Large-Area Subwavelength Hole Arrays. *Nano Lett.* **2005**, *5*, 1963–1967.
30. Yin, L.; Vlasko-Vlasov, V. K.; Rydh, A.; Pearson, J.; Welp, U.; Chang, S. H.; Gray, S. K.; Schatz, G. C.; Brown, D. B.; Kimball, C. W. Surface Plasmons at Single Nanoholes in Au Films. *Appl. Phys. Lett.* **2004**, *85*, 467–469.
31. Liu, Z. W.; Steele, J. M.; Srituravanich, W.; Pikus, Y.; Sun, C.; Zhang, X. Focusing Surface Plasmons with a Plasmonic Lens. *Nano Lett.* **2005**, *5*, 1726–1729.
32. Johnston, M. B. Superfocusing of Terahertz Waves. *Nat. Photon.* **2007**, *1*, 14–15.
33. Babadjanyan, A. J.; Margaryan, N. L.; Nerkararyan, K. V. Superfocusing of Surface Polaritons in the Conical Structure. *J. Appl. Phys.* **2000**, *87*, 3785–3788.
34. Maier, S. A.; Andrews, S. R.; Martin-Moreno, L.; Garcia-Vidal, F. J. Terahertz Surface Plasmon-Polariton Propagation and Focusing on Periodically Corrugated Metal Wires. *Phys. Rev. Lett.* **2006**, *97*, 176805-1–176805-4.
35. Stockman, M. I. Nanofocusing of Optical Energy in Tapered Plasmonic Waveguides. *Phys. Rev. Lett.* **2004**, *93*, 137404-1–137404-4.
36. Zhao, J.; Pinchuk, A. O.; McMahon, J. M.; Li, S. Z.; Ausman, L. K.; Atkinson, A. L.; Schatz, G. C. Methods for Describing the Electromagnetic Properties of Silver and Gold Nanoparticles. *Acc. Chem. Res.* **2008**, *41*, 10.1021/ar800028j.